




## Machine learning guided discovery of superconducting calcium borocarbides

Chao Zhang <sup>1</sup>, Hui Tang,<sup>1</sup> Chen Pan,<sup>1</sup> Hong Jiang,<sup>1</sup> Huai-Jun Sun <sup>2</sup>, Kai-Ming Ho,<sup>3</sup> and Cai-Zhuang Wang <sup>3,4,\*</sup>

<sup>1</sup>Department of Physics, Yantai University, Yantai 264005, China

<sup>2</sup>Jiyang College of Zhejiang Agriculture and Forestry University, Zhuji 311800, China

<sup>3</sup>Department of Physics and Astronomy, Iowa State University, Ames, Iowa 50011, USA

<sup>4</sup>Ames National Laboratory, Ames, Iowa 50011, USA



(Received 16 January 2023; revised 3 July 2023; accepted 14 July 2023; published 26 July 2023)

Pursuit of superconductivity in light-element systems at ambient pressure is of great experimental and theoretical interest. In this work, we combine a machine learning (ML) method with first-principles calculations to efficiently search for the energetically favorable ternary Ca-B-C compounds. Three layered borocarbides (stable  $\text{CaBC}_5$  and metastable  $\text{Ca}_2\text{BC}_{11}$  and  $\text{CaB}_3\text{C}_3$ ) are predicted to be phonon-mediated superconductors at ambient pressure. The stable  $\text{CaBC}_5$  and the low-energy metastable  $\text{Ca}_2\text{BC}_{11}$  (with formation energy only 9.5 meV/atom above the convex hull) have a superconducting  $T_c$  of 5.2 and 8.9 K, respectively. While the hexagonal  $\text{CaB}_3\text{C}_3$  possesses a  $T_c$  of 26.1 K, it is metastable with formation energy of 153 meV/atom above the convex hull. The ML-guided approach opens up a way for greatly accelerating the discovery of new high- $T_c$  superconductors.

DOI: [10.1103/PhysRevB.108.024512](https://doi.org/10.1103/PhysRevB.108.024512)

### I. INTRODUCTION

Migdal-Eliashberg phonon mediated theory for superconductivity suggests that light-element compounds would be promising candidates for superconductors with high transition temperature ( $T_c$ ). In contrast to heavy-element compounds in which the energy scale of phonons is usually much smaller than that of electrons, light-element materials tend to have high-frequency phonons (owing to their light atomic mass) and offer a unique playground for nontrivial interplay between the Coulomb correlations and electron-phonon interactions [1,2]. Pressurized hydrides have been predicted and observed to have high  $T_c$  above 200 K, however, most of the high- $T_c$  hydrides are synthesized and stabilized at high pressures (>100 GPa) [3–7]. Since the requirement of very high pressures would hinder the practical applications, the pursuit of a high- $T_c$  superconductor that can persist in stable or metastable compounds at or near ambient pressure has generated considerable recent interest [8], yet remains an outstanding challenge [9–11].

Boron and/or carbon compounds would be good candidates for high- $T_c$  superconductors at ambient pressure. The well-known superconducting  $\text{MgB}_2$  possesses a  $T_c$  of 39 K [12], due to strong coupling between  $\sigma$ -bonding electrons and B-B in-plane stretching vibrational phonons [13–18]. Superconductivity was also found in graphite intercalated compounds (GICs), but the  $T_c$  is generally low (< 2 K) [19], except for  $\text{CaC}_6$  which exhibits the highest  $T_c$  of 11.5 K in this class of materials [20,21]. Isovalent with and structurally similar to  $\text{MgB}_2$ , hole-doped layered  $\text{Li}_x\text{BC}$  was suggested as a high- $T_c$  superconductor [22,23]. However, superconducting  $\text{Li}_x\text{BC}$  has not been observed in experiments due to doping caused strong lattice distortion and considerable changes in

electronic band structures [24–27]. It was thus proposed that substituting carbon atoms with boron atoms would introduce hole doping in LiBC while retaining the stability of the lattice. First-principles calculations suggested that layered  $\text{Li}_3\text{B}_4\text{C}_2$ ,  $\text{Li}_2\text{B}_3\text{C}$ ,  $\text{LiB}_{1.1}\text{C}_{0.9}$ , and  $\text{Li}_4\text{B}_5\text{C}_3$  are superconductors with strong electron-phonon coupling. Moreover, alkaline earth metal intercalated layered compounds  $\text{XBC}$  ( $X = \text{Mg}, \text{Ca}, \text{Sr}, \text{Ba}$ ), which adopt LiBC structure [28], and layered  $\text{CaB}_3\text{C}_3$ , which is structurally similar to  $\text{CaC}_6$  [29], were also predicted to be phonon-mediated superconductors.

Apart from layered metal-intercalated borocarbide compounds, superconductivity was also found in carbon-boron clathrates. A carbon-boron clathrate  $\text{SrB}_3\text{C}_3$ , which was successfully synthesized at a pressure of 57 GPa [30], was theoretically predicted to be a superconductor with  $T_c \sim 40$  K [31,32]. This clathrate is composed of a single truncated octahedral B-C cage with Sr atoms incorporated at the void of the B-C cage. The electron-phonon coupling in the clathrate  $\text{SrB}_3\text{C}_3$  comes from the  $sp^3$ -hybridized  $\sigma$  bands and the boron-associated  $E_g$  phonon modes. The  $T_c$  was further enhanced to 75 K when partially substituting Sr with Rb [33,34]. By replacing the Sr atom in the clathrate  $\text{SrB}_3\text{C}_3$  with the first 57 elements ( $Z = 1-57$ ),  $\text{CaB}_3\text{C}_3$ ,  $\text{YB}_3\text{C}_3$ , and  $\text{LaB}_3\text{C}_3$  clathrates were predicted to be stable at ambient pressure [34]. High-throughput first-principles calculations of  $\text{XYB}_6\text{C}_6$  ( $X$  and  $Y$  are electropositive metal atoms) with clathrate structure find 22 dynamically stable compounds at ambient pressure and  $\text{KPbB}_6\text{C}_6$  is predicted to be a superconductor with  $T_c \sim 88$  K [35]. In addition, the B-C framework clathrates with nonequivalent B:C ratios were investigated [36].

There is only one stoichiometric calcium borocarbide,  $\text{CaB}_2\text{C}_2$ , synthesized so far for the Ca-B-C ternary system. The crystal structure of  $\text{CaB}_2\text{C}_2$  was identified to be isostructural to  $\text{LaB}_2\text{C}_2$  [37]. Subsequent studies using the x-ray diffraction method proposed that two structures with space groups,  $I4/mcm$  and  $P4/mbm$ , respectively, would be the

\*Corresponding author: wangcz@ameslab.gov

ground state of  $\text{CaB}_2\text{C}_2$  [38,39]. In fact, the total energies of the two structures are very similar using first-principles calculations [39]. The  $I4/mcm$  phase was finally determined to be the ground state of  $\text{CaB}_2\text{C}_2$  using electron energy-loss spectroscopy [40]. However, neither the  $I4/mcm$  nor the  $P4/mbm$  phase of  $\text{CaB}_2\text{C}_2$  is a superconductor. Whether there are stable compounds with high  $T_c$  in the Ca-B-C system at ambient pressure remains an open question.

In this work, we take the Ca-B-C ternary system as a prototype alkaline earth borocarbide to predict ternary compounds using an efficient framework which integrates machine learning (ML) and first-principles calculations [41,42]. Three stable and three low-energy metastable structures of calcium borocarbide are found and three of them ( $\text{CaBC}_5$ ,  $\text{Ca}_2\text{BC}_{11}$ , and  $\text{CaB}_3\text{C}_3$ ) are predicted to be phonon-mediated superconductors.

## II. COMPUTATIONAL DETAILS

The low-energy structures and compositions of the Ca-B-C system are explored using an interactive framework which combines an efficient ML model for high-throughput screening and first-principles methods for accurate calculations.

A crystal graph conventional neural network (CGCNN) ML model [43] is employed to perform the fast high-throughput screening over a wide range of possible compositions and crystal structures to select promising candidates for low-energy Ca-B-C ternary compounds. The CGCNN ML model is built on top of a crystal graph, which consists of convolutional layers and pooling layers. Crystal structures are converted to graphs with nodes and edges. Nodes represent atoms in the unit cell and are characterized by feature vector using nine measurements of atomic information, i.e., group number, period number, covalent radius, electronegativity, valence electrons, electron affinity, first ionization energy, atomic volume, and block ( $s$ ,  $p$ ,  $d$ ,  $f$ ). Edges represent atom connections which are characterized feature vectors corresponding to bonding connecting in crystal. The CGCNN ML model in Ref. [43] was obtained using structures and properties calculated by DFT and provided by Materials Project (MP) [44]. It has been shown that the CGCNN ML model can predict eight different properties of crystals, including formation energy, total energy, and band gap [43].

We construct a hypothetical structure pool for ternary Ca-B-C compounds by collecting 11 914 known ternary structures from the MP database [44] and replacing the three elements with Ca, B, and C. For a given ternary structure from the MP database, five hypothetical lattices are generated by uniformly changing the original volume by a factor of 0.96–1.04 with an interval of 0.02. There are six ways to shuffle the three elements on a given template ternary structure. Thus, a set of 357 420 hypothetical Ca-B-C structures are generated based on MP database (we refer to these structures as MP-based structures). We also generate another set of 65 287 structures using a random generation algorithm (referred to as RS-based structures) [45].

By applying the CGCNN model developed by Xie and Grossman [43] (we refer to this as the 1G-CGCNN model) to the MP-based and RS-based Ca-B-C ternary structures generated above, we select only 1200 and 1200 structures with

negative formation energies from MP-based and RS-based methods, respectively, for subsequent first-principles calculations. The results of the first-principles calculation on these 2400 candidate structures will be used to retrain the CGCNN model (referred to as the 2G-CGCNN model) to improve the accuracy specifically for the Ca-B-C system.

In order to generate sufficient data for training the 2G-CGCNN model, we also performed high-throughput first-principles calculations by substituting alkali and alkaline metals by Ca in the known stable alkali and alkaline metal borides, carbides, and borocarbides. We found some stable and metastable Ca-B binary, Ca-C binary, and Ca-B-C ternary compounds, i.e.,  $P6_3/mmc\text{-CaB}_2$ ,  $P4/mbm\text{-CaB}_3$ ,  $Imma\text{-CaB}_7$ ,  $R\bar{3}m\text{-CaC}_2$ ,  $P6/mmm\text{-CaC}_8$ ,  $P6/mmm\text{-CaC}_{12}$ ,  $Imma\text{-CaB}_{12}\text{C}_2$ , and  $P\bar{4}n2\text{-Ca}_2\text{B}_{24}\text{C}$ . For each crystalline structure of the stable and metastable Ca-B, Ca-C, and Ca-B-C compounds, we uniformly expand or contract the unit cell of the structure by a scaling factor ranging 0.85–1.25 with a 0.05 interval, and at the same time the atomic positions in each unit cell are perturbed randomly for 50 times with distortion amplitudes in the range  $-0.025$ – $0.025$  times the length of the cell vector. In this way, 4896 distorted crystalline structures are generated (referred to as DC-based structures) and the total energies of the structures are calculated by first-principles calculations.

Based on the first-principles calculation results on the 7296 structures from the three different generation methods discussed above, we select 6271 structures whose formation energies are smaller than 2 eV/atom to train the 2G-CGCNN model specifically for the Ca-B-C system. We then apply the 2G-CGCNN ML model to the set of 357 420 MP-based structures and to the set of 65 287 RS-based structures. A total of 2000 structures with low formation energy predicted by the 2G-CGCNN model from the structure pool generated by MP and RS methods are then selected for the structure relaxation by first-principles calculations. The distribution of the formation energies of hypothetical structures predicted by the 1G- and 2G-CGCNN models are given in the Supplemental Material [46].

The first-principles calculations are carried out according to DFT within the framework of the all-electron projector-augmented wave (PAW) method [47], as implemented in the Vienna Ab initio Simulation Package (VASP) [48]. We adopt the Perdew-Burk-Ernzerhof (PBE) functionals at the generalized gradient approximation (GGA) level [49]. A plane wave basis set with a kinetic energy cutoff of 520 eV is used as well as a uniform,  $\Gamma$ -centered  $k$  mesh with  $2\pi \times 0.03 \text{ \AA}^{-1}$  spacing. The electron-phonon coupling (EPC) is calculated using the QUANTUM ESPRESSO (QE) code [50] with the PBE functional and PAW pseudopotentials. The plane-wave basis set and the charge density are expanded with the kinetic energy cutoffs of 60 and 600 Ry, respectively, in the EPC calculations.

## III. RESULTS AND DISCUSSION

In order to assess the reliability of the CGCNN predictions, we randomly select 500 structures from the train database, and compare the predicted formation energies from the 1G- and 2G-CGCNN ML models with those from first-principles calculations. The performance of the 2G-CGCNN ML model

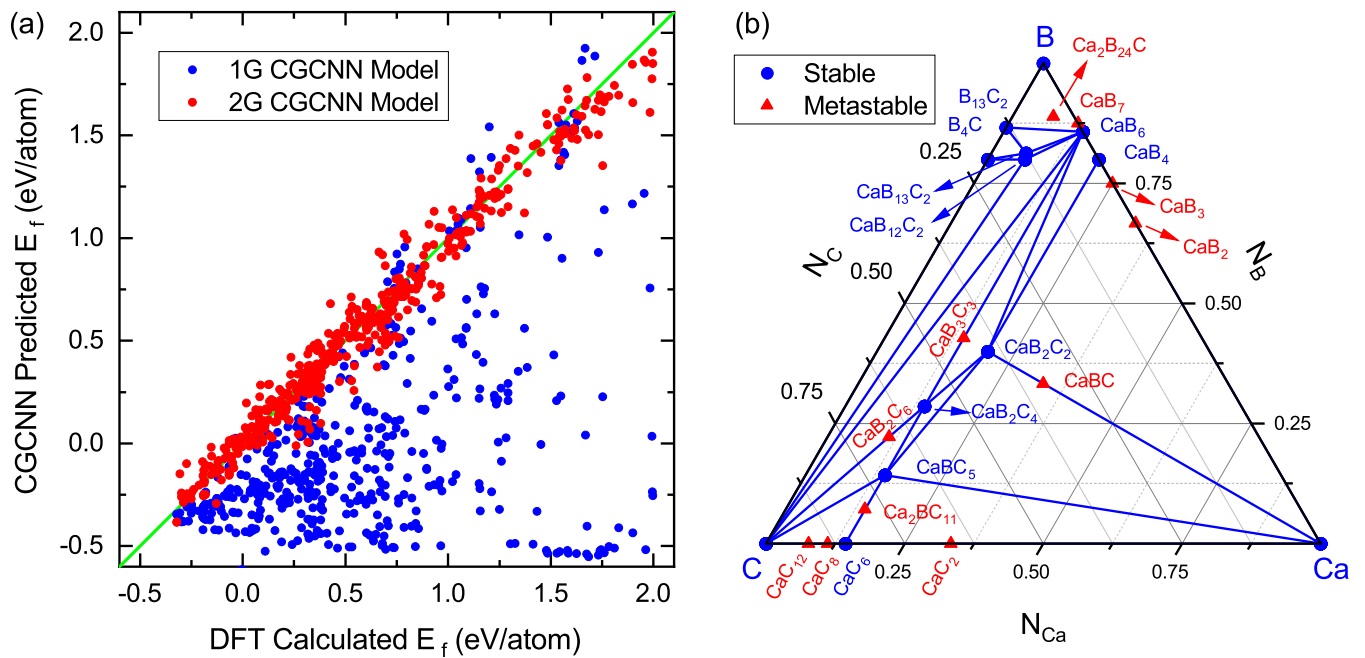


FIG. 1. (a) Formation energy of Ca-B-C system predicted by CGCNN models are compared with those from DFT. (b) Ternary phase diagram of Ca-B-C system at ambient pressure.

is significantly better than that of the 1G-CGCNN model, as shown in Fig. 1(a). The 1G-CGCNN ML model significantly underestimates the formation energies of the Ca-B-C system. The root mean square error (RMSE) of the 2G-CGCNN model is 0.092 eV/atom, which is much smaller than 0.765 eV/atom from the 1G-CGCNN model. Thus, our trained 2G-CGCNN model is more suitable for the Ca-B-C system.

The 2G-CGCNN model enables us to discover two stable calcium borocarbides,  $CaBC_5$  with *Amm2* symmetry and  $CaB_{13}C_2$  with *C2/m* symmetry. Based on  $CaBC_5$ , we build  $Ca_2BC_{11}$  with *Amm2* symmetry,  $CaB_2C_4$  with *Amm2* symmetry, and  $CaB_3C_3$  with *P6̄2m* symmetry. The structural relationships between  $CaBC_5$ ,  $Ca_2BC_{11}$ ,  $CaB_2C_4$ , and  $CaB_3C_3$  will be discussed below. The ternary phase diagram of the Ca-B-C system at ambient pressure is constructed using previously reported experimental structures

and our predicted structures, as shown Fig. 1(b). *Amm2*- $CaBC_5$ , *Amm2*- $CaB_2C_4$ , *I4/mcm*- $CaB_2C_2$ , *Imma*- $CaB_{12}C_2$ , and *C2/m*- $CaB_{13}C_2$  are stable ternary compounds. *Amm2*- $Ca_2BC_{11}$ , *Fmm2*- $CaB_2C_6$ , *P6̄2m*- $CaB_3C_3$ , *P4̄n2*- $Ca_2B_{24}C$ , *P6\_3/mmc*- $CaBC$  are metastable ternary compounds, whose formation energies are 9.5, 41.6, 153.0, 168.6, and 201.4 meV/atom, respectively, above the convex hull. To gain insight into the effects of temperature on the stable and metastable compounds, we evaluated the Gibbs free energy as a function of temperature, as shown in the Supplemental Material [46]. The ternary phase diagram of the Ca-B-C system changes slightly below 500 K, and we selected a phase diagram at 300 K, shown in the Supplemental Material [46].

Figure 2 shows the crystal structure of  $Ca_2BC_{11}$ ,  $CaBC_5$ ,  $CaB_2C_4$ , and  $CaB_3C_3$ . Similar to GICs, these four compounds are Ca intercalated layered structures. Carbon and

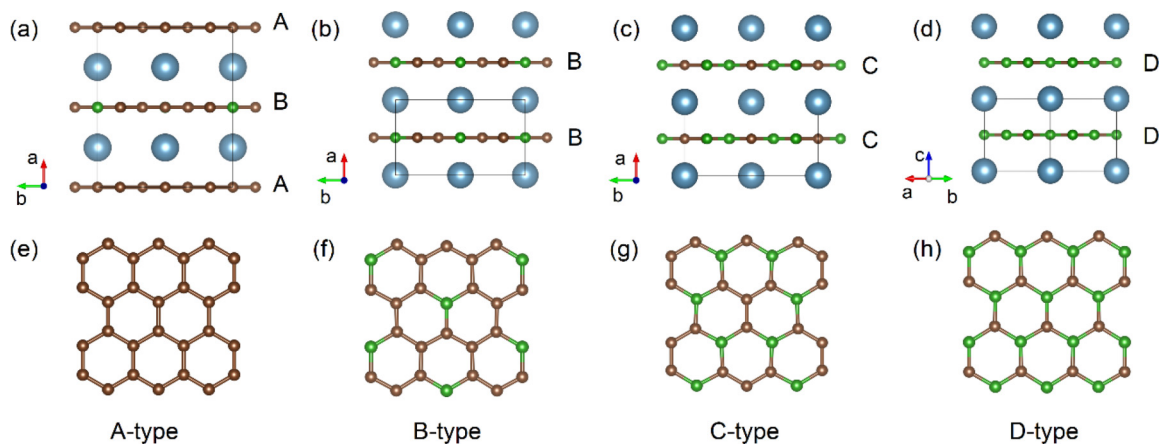


FIG. 2. Side view of crystal structures of (a)  $Ca_2BC_{11}$ , (b)  $CaBC_5$ , (c)  $CaB_2C_4$ , and (d)  $CaB_3C_3$ . (e) Graphene layer and (f)–(h) boron-carbon layers. Dark blue, green, and brown balls represent Ca, B, and C atoms, respectively.

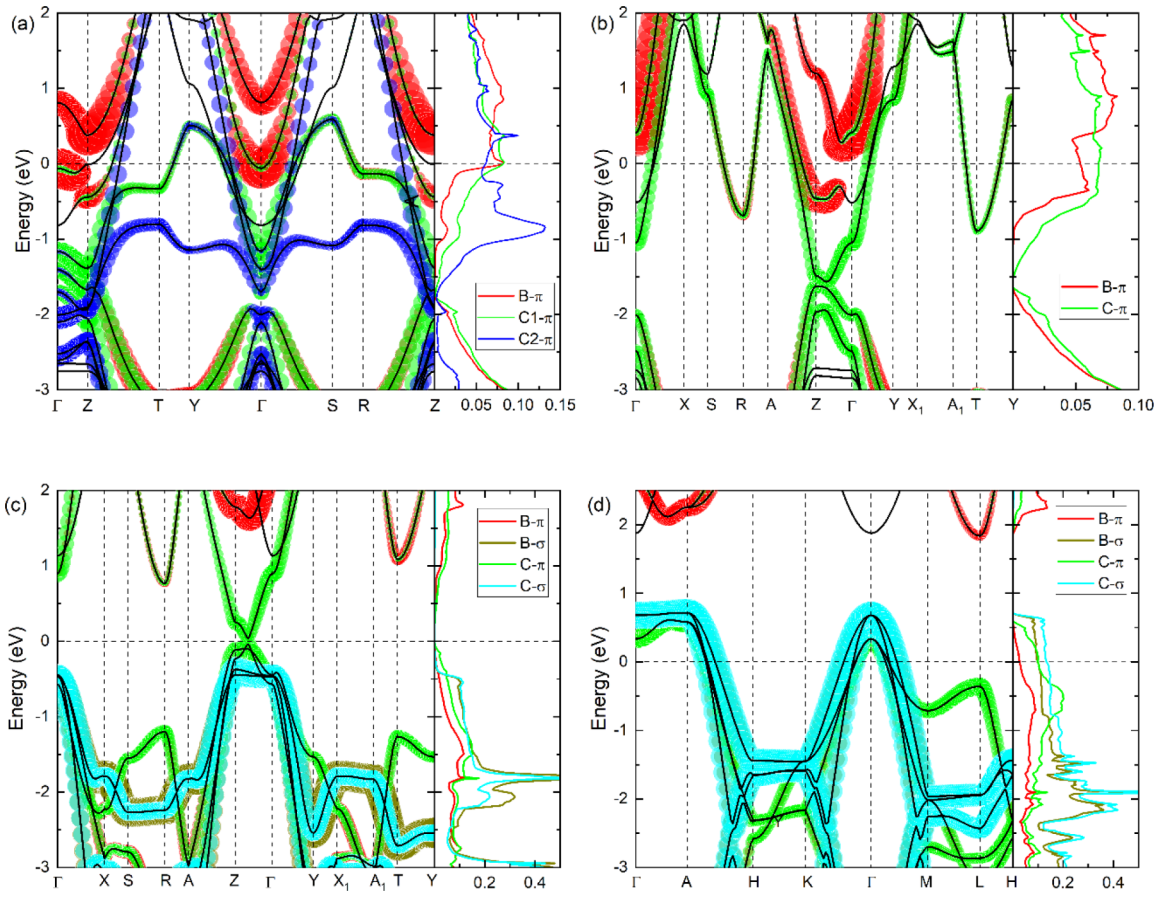


FIG. 3. Orbital-resolved electronic band structure and projected density of states (PDOS) of (a)  $\text{Ca}_2\text{BC}_{11}$ , (b)  $\text{CaBC}_5$ , (c)  $\text{CaB}_2\text{C}_4$ , and (d)  $\text{CaB}_3\text{C}_3$ . The unit of electronic PDOS is states/eV/atom.

boron atoms form three types of graphenelike layers, which are termed *B*-type (denoted as *B*), *C*-type (denoted as *C*), and *D*-type (denoted as *D*) carbon-boron layer with increasing boron content, as shown in Figs. 2(f)–2(h). The pristine graphene layer is termed an *A*-type layer (denoted as *A*), as shown in Fig. 2(e). The intercalant Ca atoms form a triangular array between graphene layers or graphenelike carbon-boron layers, and each layer of Ca intercalation is denoted as  $\alpha$ . The stacking sequences of  $\text{Ca}_2\text{BC}_{11}$ ,  $\text{CaBC}_5$ ,  $\text{CaB}_2\text{C}_4$ , and  $\text{CaB}_3\text{C}_3$  are thus in the pattern of  $A\alpha B\alpha$ ,  $B\alpha B\alpha$ ,  $C\alpha C\alpha$ , and  $D\alpha D\alpha$ , respectively. In this way,  $\text{Ca}_2\text{BC}_{11}$ ,  $\text{CaBC}_5$ , and  $\text{CaB}_2\text{C}_4$  adopt orthorhombic structures with  $\text{Amm}2$  symmetry, whereas  $\text{CaB}_3\text{C}_3$  forms a hexagonal structure with  $P\bar{6}2m$  symmetry.

Ca atoms are exactly in the middle of the adjacent boron-carbon layers in  $\text{CaBC}_5$ ,  $\text{CaB}_2\text{C}_4$ , and  $\text{CaB}_3\text{C}_3$ , while Ca atoms are biased towards the graphene layer in  $\text{Ca}_2\text{BC}_{11}$  which contains both a graphene layer and a boron-carbon layer. The average C-C bond length in the graphene layer of  $\text{Ca}_2\text{BC}_{11}$  is 1.467 Å, which is slightly larger than that of 1.449 Å in  $\text{CaC}_6$ . For  $\text{Ca}_2\text{BC}_{11}$ ,  $\text{CaBC}_5$ , and  $\text{CaB}_2\text{C}_4$  with the same  $\text{Amm}2$  symmetry, the interlayer distance between the Ca layer and the boron-carbon layer decreases with increasing content of boron. As a result, the average C-C and B-C bond lengths in the boron-carbon layer slightly increase from  $\text{Ca}_2\text{BC}_{11}$ ,  $\text{CaBC}_5$ , to  $\text{CaB}_2\text{C}_4$ . When the boron content increases to the same level of carbon in  $\text{CaB}_3\text{C}_3$ , the boron and carbon

atoms form a uniform boron-carbon layer with an average B-C bond length of 1.561 Å, as shown in Fig. 2(h). The interlayer distance between the Ca layer and the boron-carbon layer for  $\text{CaB}_3\text{C}_3$  sits between that for  $\text{CaBC}_5$  and  $\text{CaB}_2\text{C}_4$ . It is noteworthy that the stoichiometric  $\text{CaB}_3\text{C}_3$  with  $P\bar{6}2m$  symmetry predicted in this work has very similar energy with another  $\text{CaB}_3\text{C}_3$  with  $R32$  symmetry which was proposed by Chen [29]. However, the symmetry of  $P\bar{6}2m$ - $\text{CaB}_3\text{C}_3$  is higher than that of  $R32$ - $\text{CaB}_3\text{C}_3$ . In addition, the metastable  $\text{Ca}_2\text{B}_{24}\text{C}$ , stable  $\text{CaB}_{13}\text{C}_2$ , and stable  $\text{CaB}_{12}\text{C}_2$  contain B cages, and details of structural properties of these compounds are shown in the Supplemental Material [46].

The orbital-resolved electronic band structures and projected density of states (PDOS) of  $\text{Ca}_2\text{BC}_{11}$ ,  $\text{CaBC}_5$ ,  $\text{CaB}_2\text{C}_4$ , and  $\text{CaB}_3\text{C}_3$  are plotted in Fig. 3. The  $\text{Amm}2$ - $\text{Ca}_2\text{BC}_{11}$ ,  $\text{Amm}2$ - $\text{CaBC}_5$ , and  $P\bar{6}2m$ - $\text{CaB}_3\text{C}_3$  are metallic, whereas the  $\text{Amm}2$ - $\text{CaB}_2\text{C}_4$  is a semiconductor. We focus on the electronic contributions of boron and carbon atoms around the Fermi level, and the total DOS and PDOS of Ca are shown in the Supplemental Material [46]. For the  $\text{Amm}2$ - $\text{Ca}_2\text{BC}_{11}$  and  $\text{Amm}2$ - $\text{CaBC}_5$ , the  $\pi$  electrons from B and C atoms play a vital role at the Fermi level compared with  $\sigma$  electrons from them. As one can see from Figs. 3(a) and 3(b), the  $\pi$  electrons from both boron and carbon in these two structures provide significant DOS at the Fermi level. The PDOS from the  $\pi$  electrons in the mixed B-C layer decreases quickly below the Fermi level and reaches almost zero at about 1.5

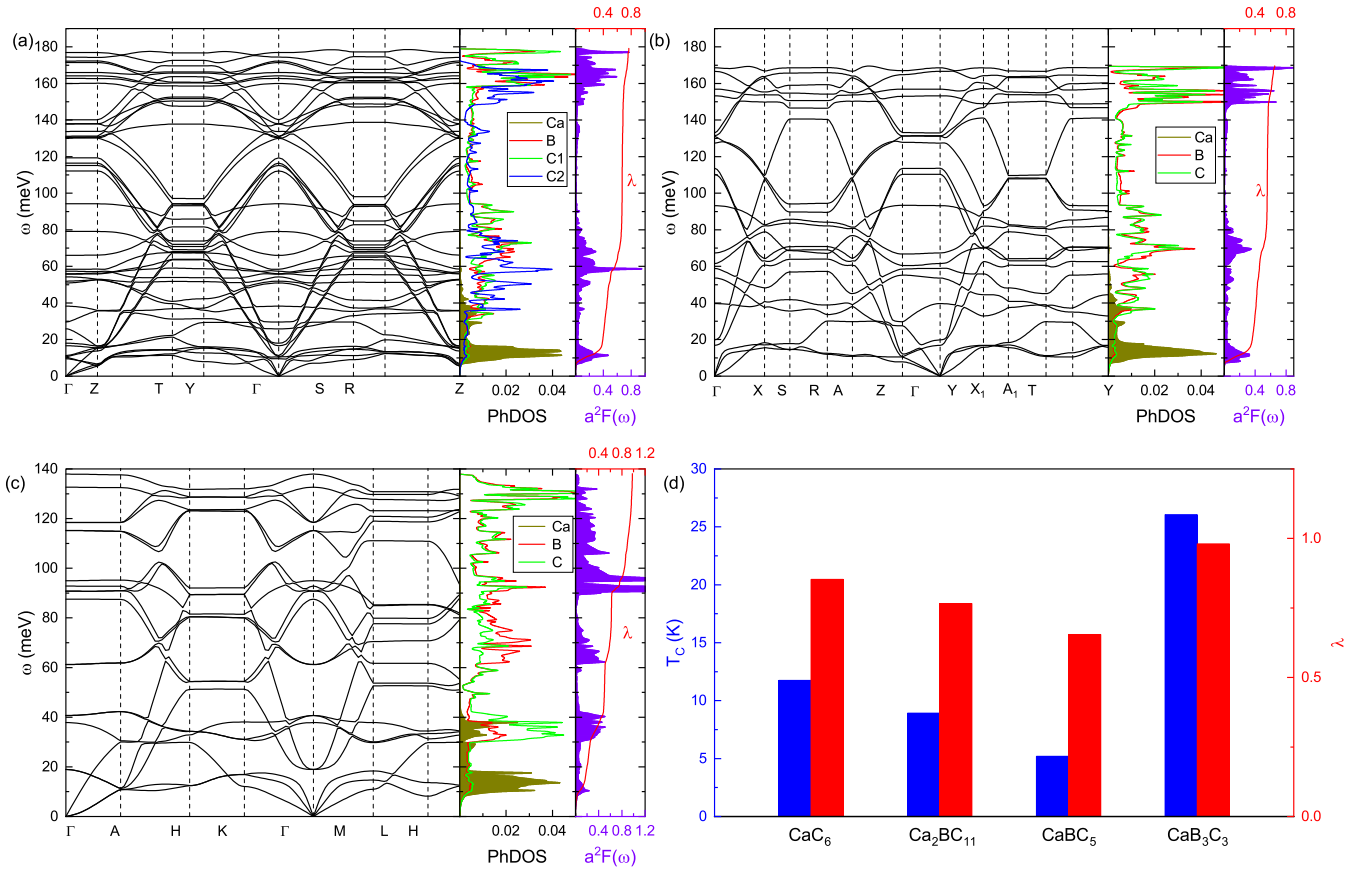


FIG. 4. Phonon band structure, phonon PDOS,  $\alpha^2F(\omega)$ , and frequency-dependent integrated  $\lambda(\omega)$  of (a)  $\text{Ca}_2\text{BC}_{11}$ , (b)  $\text{CaBC}_5$ , and (c)  $\text{CaB}_3\text{C}_3$ . (d)  $T_c$  and  $\lambda$  of  $\text{CaC}_6$ ,  $\text{Ca}_2\text{BC}_{11}$ ,  $\text{CaBC}_5$ , and  $\text{CaB}_3\text{C}_3$ .

eV below the Fermi level, while the PDOS of the  $\pi$  electrons from the graphene layer in the  $\text{Amm}2\text{-Ca}_2\text{BC}_{11}$  increases and forms a peak around 1 eV below the Fermi level combined with Ca  $d$  states, as shown in the Supplemental Material [46]. Different from  $\text{Amm}2\text{-Ca}_2\text{BC}_{11}$  and  $\text{Amm}2\text{-CaBC}_5$ , the  $\sigma$  electrons from B and C atoms in the  $\text{Amm}2\text{-CaB}_2\text{C}_4$  and  $\text{P}\bar{6}2m\text{-CaB}_3\text{C}_3$  structures play an important role in the PDOS around the Fermi level. The top of the valence band and the bottom of the conduction band of  $\text{Amm}2\text{-CaB}_2\text{C}_4$  locate between the  $Z \rightarrow \Gamma$  line, which results in a small gap of 0.08 eV at the PBE level. The  $\text{P}\bar{6}2m\text{-CaB}_3\text{C}_3$  is metallic with strong contributions from the  $\sigma$  electrons of boron and carbon atoms to the states at the Fermi level in addition to the  $\pi$  electron contributions, although there is a band gap of  $\sim 1$  eV that starts from about 0.7 eV above the Fermi level. The band structure of this structure exhibits a combination of some flat bands and some steep bands in the vicinity of the Fermi level along the  $\Gamma \rightarrow A$  direction. The simultaneous occurrence of flat and steep bands near the Fermi level has been suggested as essential to superconducting behavior. In addition, the B-rich ternary compounds ( $\text{Imma}\text{-CaB}_{12}\text{C}_2$ ,  $\text{C}2/m\text{-CaB}_{13}\text{C}_2$ , and  $\text{P}4n2\text{-Ca}_2\text{B}_{24}\text{C}$ ) show semiconducting characteristics. The band gaps of  $\text{C}2/m\text{-CaB}_{13}\text{C}_2$ ,  $\text{Imma}\text{-CaB}_{12}\text{C}_2$ , and  $\text{P}4n2\text{-Ca}_2\text{B}_{24}\text{C}$  are 0.80, 1.41, and 1.82 eV, respectively. Details of the electronic band structures of newly predicted B-rich compounds are shown in the Supplemental Material [46].

Figure 4 presents the phonon band structure, phonon PDOS, Eliashberg spectral function  $\alpha^2F(\omega)$ , and integrated electron-phonon coupling constant  $\lambda(\omega)$  of the  $\text{Amm}2\text{-Ca}_2\text{BC}_{11}$ ,  $\text{Amm}2\text{-CaBC}_5$ , and  $\text{P}\bar{6}2m\text{-CaB}_3\text{C}_3$ . The absence of imaginary of phonon frequencies establishes the dynamical stabilities of these predicted structures. For the three compounds, the low-frequency range (below 20 meV) is dominated by Ca atoms and the vibration of Ca atoms extends to 60 meV. The frequency range above 60 meV is dominated by B and C atoms.  $\text{Amm}2\text{-Ca}_2\text{BC}_{11}$  and  $\text{Amm}2\text{-CaBC}_5$  have similar distributions of the Eliashberg spectral function, which leads to three steps in the integrated  $\lambda(\omega)$ . The vibration of Ca atoms mainly contributes to the first step of the integrated  $\lambda(\omega)$ , which are 51.8% and 55.6% of the total  $\lambda$  for  $\text{Amm}2\text{-Ca}_2\text{BC}_{11}$  and  $\text{Amm}2\text{-CaBC}_5$ , respectively. The intermediate-frequency range (20–100 meV) and high-frequency range (150–180 meV) approximately contribute to 30% and 10% the total  $\lambda$ , respectively. The distribution of the Eliashberg spectral function of  $\text{P}\bar{6}2m\text{-CaB}_3\text{C}_3$  is apparently different from that of  $\text{Amm}2\text{-Ca}_2\text{BC}_{11}$  and  $\text{Amm}2\text{-CaBC}_5$ . There are four steps in the integrated  $\lambda(\omega)$ . The low-frequency range (0–20 meV) dominated by Ca atoms only contributes 20.2% to the total  $\lambda$ . The frequency range located at 20–60 meV, which reflects strong interaction between Ca, B, and C atoms, contributes 31.9% to the total  $\lambda$ . The high-frequency range (80–140 meV) coming from B and C atoms contributes 36.9% to the total  $\lambda$ . Especially, the phonon vibration

around 90 meV strongly couples with  $\sigma$  electrons of B and C atoms.

We estimate the  $T_c$  of the Ca-B-C system at ambient pressure using the Allen-Dynes modified version of the McMillan equation [51,52]:

$$T_c = \frac{\omega_{\log}}{1.2} \exp \left[ -\frac{1.04(1 + \lambda)}{\lambda - \mu^*(1 + 0.62\lambda)} \right].$$

By taking  $\mu^* = 0.15$ , we find that the  $T_c$  of  $R\bar{3}m$ -CaC<sub>6</sub> is 11.7 K which is in excellent consistency with the experimental data (11.5 K) [20] and previously theoretical value (9.4 K) using the anisotropic Migdal-Eliashberg method [53]. Moreover, for a theoretically predicted metal borocarbide Li<sub>3</sub>B<sub>4</sub>C<sub>2</sub>, the value of  $T_c$  calculated from the McMillan method (53.8 K) coincides with that from the anisotropic Migdal-Eliashberg method (53.9 K) [54]. Thus, the McMillan method estimates  $T_c$  reasonably well for the Ca-B-C system. The  $T_c$ 's of  $R\bar{3}m$ -CaC<sub>6</sub>,  $Amm2$ -Ca<sub>2</sub>BC<sub>11</sub>,  $Amm2$ -CaBC<sub>5</sub>, and  $P\bar{6}2m$ -CaB<sub>3</sub>C<sub>3</sub> using  $\mu^* = 0.15$  are shown in Fig. 4(d). With increasing B contents from the  $R\bar{3}m$ -CaC<sub>6</sub>, the  $Amm2$ -CaBC<sub>11</sub>, to the  $Amm2$ -CaBC<sub>5</sub>, the  $\lambda$  monotonically decreases from 0.853 to 0.766 and to 0.655. Correspondingly,  $T_c$  decreases from 11.8 to 8.9 and to 5.2 K. This comes from the similar Eliashberg distributions of these three compounds.  $P\bar{6}2m$ -CaB<sub>3</sub>C<sub>3</sub> possesses the largest  $T_c$  (26.1 K) among the four compounds. The high  $T_c$  stems from the strong coupling between  $\sigma$  bonding and B and C vibration in the frequency range 87–95 meV. It is worth noting that the  $T_c$  of  $R32$ -CaB<sub>3</sub>C<sub>3</sub> is estimated to be 26.7 K, which is in agreement with the  $T_c$  of 28.2 K obtained by Chen [29]. In addition, we explore the effect of Coulomb pseudopotential  $\mu^*$  on the  $T_c$  of the four calcium borocarbides, as shown in Fig. S8 [46]. As shown in Fig. S8, the  $T_c$  values of the four compounds increase with decreasing  $\mu^*$ . Using  $\mu^* = 0.10$ , the values of  $T_c$  of  $R\bar{3}m$ -CaC<sub>6</sub>,  $Amm2$ -Ca<sub>2</sub>BC<sub>11</sub>,  $Amm2$ -CaBC<sub>5</sub>, and  $P\bar{6}2m$ -CaB<sub>3</sub>C<sub>3</sub> reach 16.5, 13.3, 8.81, and 34.2 K, respectively.

#### IV. CONCLUSIONS

In summary, we search for low-energy Ca-B-C ternary compounds using an efficient framework which combines ML high-throughput screening with accurate first-principles calculations and explore the possible superconductivity of these compounds at ambient pressure. Four stable ( $Amm2$ -CaBC<sub>5</sub>,  $Amm2$ -CaB<sub>2</sub>C<sub>4</sub>,  $Imma$ -CaB<sub>12</sub>C<sub>2</sub>, and  $C2/m$ -CaB<sub>13</sub>C<sub>2</sub>) and three metastable ( $Amm2$ -Ca<sub>2</sub>BC<sub>11</sub>,  $P\bar{6}2m$ -CaB<sub>3</sub>C<sub>3</sub>, and  $P\bar{4}n2$ -Ca<sub>2</sub>B<sub>24</sub>C) calcium borocarbides are revealed. Layered  $Amm2$ -Ca<sub>2</sub>BC<sub>11</sub>,  $Amm2$ -CaBC<sub>5</sub>, and  $P\bar{6}2m$ -CaB<sub>3</sub>C<sub>3</sub> are predicted to be phonon-mediated superconductors. Among the three superconductors, the metastable  $P\bar{6}2m$ -CaB<sub>3</sub>C<sub>3</sub> has the highest  $T_c$  of 26.1 K, but its formation energy is 153 meV/atom above the convex hull. The stable CaBC<sub>5</sub> and the low-energy metastable Ca<sub>2</sub>BC<sub>11</sub> (with formation energy within 10 meV/atom with respect to the convex hull) have lower  $T_c$  of 5.2 and 8.9 K, respectively.  $Amm2$ -CaB<sub>2</sub>C<sub>4</sub>,  $C2/m$ -CaB<sub>13</sub>C<sub>2</sub>,  $Imma$ -CaB<sub>12</sub>C<sub>2</sub>, and  $P\bar{4}n2$ -Ca<sub>2</sub>B<sub>24</sub>C are semiconductors, which have band gaps of 0.08, 0.80, 1.41, and 1.82 eV, respectively. The stable and metastable structures of the Ca-B-C system have significant implications for alkali and alkaline metal borocarbides. The ML-guided approach opens up a way for greatly accelerating the discovery of new high- $T_c$  superconductors.

#### ACKNOWLEDGMENTS

C.Z. was supported by the National Natural Science Foundation of China (Grant No. 11874318). Work at Ames National Laboratory was supported by the US Department of Energy (DOE), Office of Science, Basic Energy Sciences, Materials Science and Engineering Division, including a grant of computer time at the National Energy Research Supercomputing Center (NERSC) in Berkeley. Ames National Laboratory is operated for the US DOE by Iowa State University under Contract No. DE-AC02-07CH11358.

- 
- [1] R. Arita, T. Koretsune, S. Sakai, R. Akashi, Y. Nomura, and W. Sano, *Adv. Mater.* **29**, 1602421 (2017).
- [2] N. W. Ashcroft, *Phys. Rev. Lett.* **21**, 1748 (1968).
- [3] N. W. Ashcroft, *Phys. Rev. Lett.* **92**, 187002 (2004).
- [4] A. P. Drozdov, M. I. Erements, I. A. Troyan, V. Ksenofontov, and S. I. Shylin, *Nature (London)* **525**, 73 (2015).
- [5] A. P. Drozdov, P. P. Kong, V. S. Minkov, S. P. Besedin, M. A. Kuzovnikov, S. Mozaffari, L. Balicas, F. F. Balakirev, D. E. Graf, V. B. Prakapenka, E. Greenberg, D. A. Knyazev, M. Tkacz, and M. I. Erements, *Nature (London)* **569**, 528 (2019).
- [6] I. A. Troyan, D. V. Semenov, A. G. Kvashnin, A. V. Sadakov, O. A. Sobolevskiy, V. M. Pudalov, A. G. Ivanova, V. B. Prakapenka, E. Greenberg, A. G. Gavriliuk, I. S. Lyubutin, V. V. Struzhkin, A. Bergara, I. Errea, R. Bianco, M. Calandra, F. Mauri, L. Monacelli, R. Akashi, and A. R. Oganov, *Adv. Mater.* **33**, 2006832 (2021).
- [7] E. Snider, N. Dasenbrock-Gammon, R. McBride, X. Wang, N. Meyers, K. V. Lawler, E. Zurek, A. Salamat, and R. P. Dias, *Phys. Rev. Lett.* **126**, 117003 (2021).
- [8] N. Dasenbrock-Gammon, E. Snider, R. McBride, H. Pasan, D. Durkee, N. Khalvashi-Sutter, S. Munasinghe, S. E. Dissanayake, K. V. Lawler, A. Salamat, and R. P. Dias, *Nature (London)* **615**, 244 (2023).
- [9] X. Ming, Y.-J. Zhang, X. Zhu, Q. Li, C. He, Y. Liu, T. Huang, G. Liu, B. Zheng, H. Yang, J. Sun, X. Xi, and H.-H. Wen, *Nature (London)* (2023), doi:10.1038/s41586-023-06162-w.
- [10] P. Shan, N. Wang, X. Zheng, Q. Qiu, Y. Peng, and J. Cheng, *Chinese Phys. Lett.* **40**, 046101 (2023).
- [11] Z. Li, X. He, C. Zhang, K. Lu, B. Min, J. Zhang, S. Zhang, J. Zhao, L. Shi, Y. Peng, S. Feng, Z. Deng, J. Song, Q. Liu, X. Wang, R. Yu, L. Wang, Y. Li, J. D. Bass, V. Prakapenka, S. Chariton, H. Liu, and C. Jin, *Sci. China: Phys., Mech. Astron.* **66**, 267411 (2023).
- [12] J. Nagamatsu, N. Nakagawa, T. Muranaka, Y. Zenitani, and J. Akimitsu, *Nature (London)* **410**, 63 (2001).
- [13] J. M. An and W. E. Pickett, *Phys. Rev. Lett.* **86**, 4366 (2001).
- [14] Y. Kong, O. V. Dolgov, O. Jepsen, and O. K. Andersen, *Phys. Rev. B* **64**, 020501(R) (2001).

- [15] T. Yildirim, O. Gülseren, J. W. Lynn, C. M. Brown, T. J. Udovic, Q. Huang, N. Rogado, K. A. Regan, M. A. Hayward, J. S. Slusky, T. He, M. K. Haas, P. Khalifah, K. Inumaru, and R. J. Cava, *Phys. Rev. Lett.* **87**, 037001 (2001).
- [16] H. J. Choi, D. Roundy, H. Sun, M. L. Cohen, and S. G. Louie, *Nature (London)* **418**, 758 (2002).
- [17] H. J. Choi, D. Roundy, H. Sun, M. L. Cohen, and S. G. Louie, *Phys. Rev. B* **66**, 020513(R) (2002).
- [18] J. Kortus, I. I. Mazin, K. D. Belashchenko, V. P. Antropov, and L. L. Boyer, *Phys. Rev. Lett.* **86**, 4656 (2001).
- [19] Y. Iye and S.-i. Tanuma, *Phys. Rev. B* **25**, 4583 (1982).
- [20] N. Emery, C. Hérold, M. d'Astuto, V. Garcia, C. Bellin, J. F. Maréché, P. Lagrange, and G. Loupiau, *Phys. Rev. Lett.* **95**, 087003 (2005).
- [21] T. E. Weller, M. Ellerby, S. S. Saxena, R. P. Smith, and N. T. Skipper, *Nat. Phys.* **1**, 39 (2005).
- [22] H. Rosner, A. Kitaigorodsky, and W. E. Pickett, *Phys. Rev. Lett.* **88**, 127001 (2002).
- [23] J. K. Dewhurst, S. Sharma, C. Ambrosch-Draxl, and B. Johansson, *Phys. Rev. B* **68**, 020504(R) (2003).
- [24] A. Bharathi, S. Jemima Balaselvi, M. Premila, T. N. Sairam, G. L. N. Reddy, C. S. Sundar, and Y. Hariharan, *Solid State Commun.* **124**, 423 (2002).
- [25] D. Souptel, Z. Hossain, G. Behr, W. Löser, and C. Geibel, *Solid State Commun.* **125**, 17 (2003).
- [26] A. M. Fogg, P. R. Chalker, J. B. Claridge, G. R. Darling, and M. J. Rosseinsky, *Phys. Rev. B* **67**, 245106 (2003).
- [27] A. M. Fogg, J. Meldrum, G. R. Darling, J. B. Claridge, and M. J. Rosseinsky, *J. Am. Chem. Soc.* **128**, 10043 (2006).
- [28] E. Haque, M. A. Hossain, and C. Stampfl, *Phys. Chem. Chem. Phys.* **21**, 8767 (2019).
- [29] W. Chen, *J. Appl. Phys.* **114**, 173906 (2013).
- [30] L. Zhu, G. M. Borstad, H. Liu, P. A. Guñka, M. Guertel, J.-A. Dolyniuk, Y. Meng, E. Greenberg, V. B. Prakapenka, B. L. Chaloux, A. Epshteyn, R. E. Cohen, and T. A. Strobel, *Sci. Adv.* **6**, eaay8361 (2020).
- [31] J.-N. Wang, X.-W. Yan, and M. Gao, *Phys. Rev. B* **103**, 144515 (2021).
- [32] L. Zhu, H. Liu, M. Somayazulu, Y. Meng, P. A. Guñka, T. B. Shiell, C. Kenney-Benson, S. Chariton, V. B. Prakapenka, H. Yoon, J. A. Horn, J. Paglione, R. Hoffmann, R. E. Cohen, and T. A. Strobel, *Phys. Rev. Res.* **5**, 013012 (2023).
- [33] P. Zhang, X. Li, X. Yang, H. Wang, Y. Yao, and H. Liu, *Phys. Rev. B* **105**, 094503 (2022).
- [34] S. Di Cataldo, S. Qulaghasi, G. B. Bachelet, and L. Boeri, *Phys. Rev. B* **105**, 064516 (2022).
- [35] N. Geng, K. P. Hilleke, L. Zhu, X. Wang, T. A. Strobel, and E. Zurek, *J. Am. Chem. Soc.* **145**, 1696 (2023).
- [36] Z. Cui, X. Zhang, Y. Sun, Y. Liu, and G. Yang, *Phys. Chem. Chem. Phys.* **24**, 16884 (2022).
- [37] J. Bauer and O. Bars, *Acta Crystallogr., Sect. B* **36**, 1540 (1980).
- [38] B. Albert and K. Schmitt, *Inorg. Chem.* **38**, 6159 (1999).
- [39] J. Akimitsu, K. Takenawa, K. Suzuki, H. Harima, and Y. Kuramoto, *Science* **293**, 1125 (2001).
- [40] K. Hofmann and B. Albert, *ChemPhysChem* **3**, 896 (2002).
- [41] W. Xia, M. Sakurai, B. Balasubramanian, T. Liao, R. Wang, C. Zhang, H. Sun, K.-M. Ho, J. R. Chelikowsky, D. J. Sellmyer, and C.-Z. Wang, *Proc. Natl. Acad. Sci. USA* **119**, e2204485119 (2022).
- [42] H. Sun, C. Zhang, W. Xia, L. Tang, R. Wang, G. Akopov, N. W. Hewage, K.-M. Ho, K. Kovnir, and C.-Z. Wang, *Inorg. Chem.* **61**, 16699 (2022).
- [43] T. Xie and J. C. Grossman, *Phys. Rev. Lett.* **120**, 145301 (2018).
- [44] A. Jain, S. P. Ong, G. Hautier, W. Chen, W. D. Richards, S. Dacek, S. Cholia, D. Gunter, D. Skinner, G. Ceder, and K. A. Persson, *APL Mater.* **1**, 011002 (2013).
- [45] P. Avery and E. Zurek, *Comput. Phys. Commun.* **213**, 208 (2017).
- [46] See Supplemental Material at <http://link.aps.org/supplemental/10.1103/PhysRevB.108.024512> for lattice parameters and atomic positions of calcium borocarbides, formation energy distribution from CGCNN ML predictions, temperature dependent Gibbs free energy, ternary phase diagram of Ca-B-C system at ambient pressure and 300 K, electronic projected density of states, crystal structures, electronic band structures, and phonon band structures of B-rich ternary compounds.
- [47] G. Kresse and D. Joubert, *Phys. Rev. B* **59**, 1758 (1999).
- [48] G. Kresse and J. Furthmüller, *Phys. Rev. B* **54**, 11169 (1996).
- [49] J. P. Perdew, K. Burke, and M. Ernzerhof, *Phys. Rev. Lett.* **77**, 3865 (1996).
- [50] P. Giannozzi, S. Baroni, N. Bonini, M. Calandra, R. Car, C. Cavazzoni, D. Ceresoli, G. L. Chiarotti, M. Cococcioni, I. Dabo, A. D. Corso, S. d. Gironcoli, S. Fabris, G. Fratesi, R. Gebauer, U. Gerstmann, C. Gougoussis, A. Kokalj, M. Lazzeri, L. Martin-Samos *et al.*, *J. Phys.: Condens. Matter* **21**, 395502 (2009).
- [51] W. L. McMillan, *Phys. Rev.* **167**, 331 (1968).
- [52] P. B. Allen and R. C. Dynes, *Phys. Rev. B* **12**, 905 (1975).
- [53] A. Sanna, G. Profeta, A. Floris, A. Marini, E. K. U. Gross, and S. Massidda, *Phys. Rev. B* **75**, 020511(R) (2007).
- [54] M. Gao, Z.-Y. Lu, and T. Xiang, *Phys. Rev. B* **91**, 045132 (2015).